



Desertification assessment using Sentinel-2A images, spectral and TCT indices in the Admer-Ezem watershed, upper Oum-Rbaa basin, Morocco

Abdelhak Limame ¹, Khalid El Hairchi ^{*2}, Lahcen Ouiaboub ³

¹ Sidi Mohamed Ben Abdellah University, geography, Morocco, Limameabdelhak@gmail.com

² Sultan Moulay Slimane University, Research team, Territory: Dynamics, Planning and Sustainable Development (TEA2D), FPK, Morocco, k.elhairchi@usms.ma

³ Ibn Tofail University, Laboratory of Territories, Environment and Development, Morocco, lahcen.ouiaboub@uit.ac.ma

Cite this study:

Limame, A., El Hairchi, K., & Ouiaboub, L. (2026). Desertification assessment using Sentinel-2A images, spectral and TCT indices in the Admer-Ezem watershed, upper Oum-Rbaa basin, Morocco. *International Journal of Engineering and Geosciences*, 11(2), 375-391.

<https://doi.org/10.26833/ijeg.1690805>

Keywords

Sentinel 2A
Spectral Index
TCT
Desertification
Morocco

Research Article

Received:03.05.2025

Revised: 28.09.2025

Accepted:10.10.2025

Published:01.07.2026



Abstract

This paper focuses on a quantitative assessment of desertification in the Admer-Ezem basin, using Sentinel-2A satellite images and indices to map the degree of basin-wide desertification in 2023. The methodology is based on the extraction of several spectral indices, such as the normalized difference vegetation index (NDVI), albedo, topsoil grain size index (TGSi) and the modified soil adjusted vegetation index (MSAVI), as well as the tasseled cap transformation (TCT) indices: brightness (TCB), greenness (TCG) and wetness (TCW). Different combinations of these indices were then created and analyzed using linear regression to identify low correlation rates. Based on these results, three characteristic zones were selected: TGSi-Albedo ($r = -0.95$), TGSi-TCW ($r = -0.74$) and TCW-TCB ($r = -0.73$). The resulting map subdivides the region into five categories of desertification: extreme, severe, moderate, low and non-desertified. The results show that the forest is undergoing progressive desertification. In general, and according to the different models used, more than 50% of the area studied is subject to severe to extreme desertification, while less than 30% of the area is classified as no-desertified, or slightly affected. Thanks to the high accuracy of the models used (Area Under the Curve (AUC) from 79 to 83%), this approach proves to be almost optimal for the quantitative analysis and monitoring of desertification in the Moroccan Middle Atlas. Finally, this work can help planners identify the most suitable sites for future forest development.

1. Introduction

Desertification is a problem that affects over a billion people globally [1-5]. The United Nations Convention to Combat Desertification [6] defines this phenomenon as the progressive land degradation in arid, semi-arid, and dry sub-humid areas thanks to a conjunction of human activities, including intensive and extensive agriculture, and climatic variations, such as high temperatures and decreased precipitation. These activities lead to overexploitation of land and exceeding its regeneration capacity [7- 8]

Desertification affects approximately 39.2% of the global land surface, or $51.6 \times 10^6 \text{ km}^2$ of degraded land [9]. North Africa alone has an area of $4.86 \times 10^6 \text{ km}^2$

affected by this phenomenon [10]. Desertification leads to serious consequences, such as biodiversity loss, habitat destruction, endangerment of plant species and a decrease in soil productivity [11-15]. It also alters the Earth surface's hydrological, ecological, and biogeochemical processes [16].

In the southern Mediterranean, Morocco is among the nation's worst affected by desertification. According to the Arab Organization for Agricultural Development (AOAD)[17], more than 64.01% of the land is already desertified, and 27.43% is threatened by this problem. This situation results from the combination of several factors, namely: the aridity of the environment (93% of the national territory), the irregularity of precipitation

and the frequency of drought [18- 19], the excessive exploitation of natural resources (water, soil, forest) following the increase in demographic pressure which generates growing food needs for the population and livestock [20]. Moreover, the deforestation of the environment which causes a regression of the forest cover of 17,000 ha/year [21], due to the excessive harvesting of firewood and energy, overgrazing, clearing and fires.

Aware being of the seriousness of the desertification phenomenon, many researchers have studied it in several Moroccan regions, using different methods and models. These Regions include the Guercif basin in eastern Morocco [22], the Souss watershed [7], the Moulouya basin [20], and the Oued El Maleh watershed [23], the Drâa basin [24], the Middle Moulouya basin [15], the Upper Oueghra and Central Rif basins [25- 26], and the Middle Atlas [27].

The authors have all concluded that Morocco is among the Mediterranean countries most impacted by these environmental phenomena, which differs depending on the location. It should be mentioned that scholars have never delved into desertification in our study area.

Numerous techniques and models have been used to assess and evaluate ecosystems hazards like desertification in order to map and evaluate this risk [28]. However, the method based on remote sensing technologies (Sentinel, ASTER, Landsat, Ikonos, Quickbird and Spot) remains the most effective [27]. This method has been in use for the past three decades [29, 30].

Remote sensing offers accurate data and statistics, rapid updating and a large amount of information [31,24]. Combined with a geographic information system (GIS), it enables rapid assessment of land characteristics and their evolution in space and time, thanks to the availability of multi-temporal and high-resolution satellite images which helps to Analysis large-scale environments [15, 32 - 33].

These geo-spatial technologies can be used either to halt the progression of desertification, or to mitigate its effects [24, 27-34]. In arid, semi-arid and dry sub-humid worldwide zones, several spectral indicators have been developed to monitor and evaluate desertification degrees [15, 24], such as the Desertification Degree Index (DDI) approach created by [35]. This model is established by combining two most inversely correlated indicators to create a feature space.

However, in several studies, authors have used different indices depending on the correlation rate. For example, [36] used the Albedo-NDVI model to assess desertification, [37] used the Albedo-MSAVI model, [38] used the Albedo-TGSI model, while the use of TCT indices by [24, 27] gave good results in Morocco.

In this paper, we will use combinations of the following spectral and TCT indices: TCW-TCB, TGSI-Albedo and TGSI-TCW, which showed good inverse correlations to monitor and assess the degree of desertification in Admer-Ezem.

Using high-resolution Sentinel 2A images, the study aims to map the extent of desertification in the upper Oum-Rbaa basin based on the outcomes of negative regression analysis and inversion of the TCT, MSAVI, TGSI, NDVI, and Albedo indices. The models developed can be extended to other arid or semi-arid zones to assess the degree of desertification in Morocco.

Study area:

Located at the summit of the large Oum-Rbaa basin, the Oued Admer-Ezem watershed spans 197.59 km², as indicated by the Lambert coordinates: X1 = 430 347.24, Y1 = 281 864.43; X2= 529 704.23, Y2 = 386 110.82. This area is limited to the north by the Sebou basin, to the west and south-west by the basin of Amengous-Fellat and to the east by the Ouiouane watershed (Figure 1).

The climate of the region is sub-humid to semi-arid, with hot summers and wet, chilly winters. Precipitation in the Tamchachat station (in Admer-Ezem) is 663.5 mm, recorded at the only weather station in Tamchachat. Additionally, the temperatures vary greatly, ranging from a summer high of 30°C to a winter low of -6°C [39-40]. The majority of the natural plant cover is quite varied: Cedar (*Cedrus atlantica*), holm oak (*Quercus rotundifolia*) and Thuya (*Tetraclinis articulata*) [41-42]. The main economic activities in the study area are pastoralism and agriculture, which put pressure on natural resources.

Geologically, the Upper Oum-Rbaa watershed is part of the central Middle Atlas and is situated in the passage zone of the North Middle Atlas accident [43]. It displays a broad range of stratigraphic sedimentary layers from the Upper Triassic to the Quaternary. The mountainous expansions of Elkoubate and Ijdrane (Ain Kahla, Mimjad, etc.) and the domes are framed by the carbonate formations (limestones and dolomites) of the Middle and Lower Lias. According to [40], the Triassic outcrops are located in the passage zone of major accidents that transverse the basin, such as the Marmal disaster from north to south and the North Middle Atlas accident from east to west. At the start of the Jurassic sedimentary outcrop, dolomites and red clays alternate, indicating the transition. At the start of the Jurassic sedimentary outcrop, dolomites and red clays alternate, indicating the change from the Upper Triassic's mostly continental sedimentation to a marine one, which is supported by carbonate deposits in the Liassic [44]. A strong calcar-dolomitic structure serves as a representation of the Lower Liassic deposits. According to [44], these deposits are nearly consistent with those of the Upper Triassic.

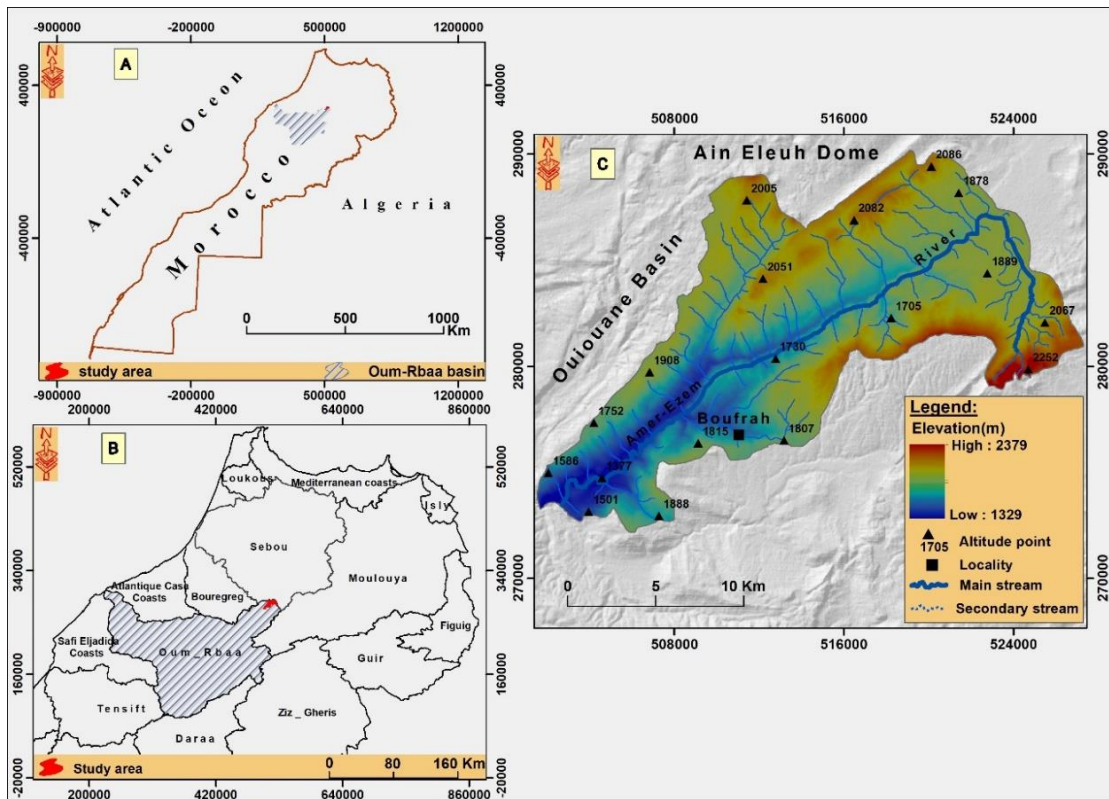


Figure 1. The study area location; A: Moroccan nation, B: Oum_Rbaa basin, C: Admer-Ezem basin

2. Materials and Methods

2.1. Data

In this study we are based on multiple and diverse data resources and software, Multispectral Sentinel-2A images have been obtained from the Copernicus website (<https://scihub.copernicus.eu>). The images were taken on August 14, 2023, during the dry season, when there is less agricultural activity, little precipitation, and low chlorophyll.

These sentinel-2A images reflect the ground truth, since the cloud cover was very low. In fact, these sentinel-2A images are composed of 13 spectral bands at different resolutions of 10 m, 20 m and 60 m (table. 1). The wavelengths covered by these 13 bands range widely, from 440 to 2200 nm. Several software programs were used for preprocessing, processing, statistical regression analysis, and presentation of results.

Table 1. Characteristics of Sentinel-2 satellite imagery

Sentinel-2 bands	Resolution	Central Wavelengths (nm)
Band 1: Coastal/aerosols	60m	0.443
Band 2: Visible Blue	10m	0.49
Band 3: Visible Green	10m	0.56
Band 4: Visible Red	10m	0.665
Band 5: Vegetation Red Edge	20m	0.705
Band 6: Vegetation Red Edge	20m	0.74
Band 7: Vegetation Red Edge	20m	0.783
Band 8: Near-Infrared	10m	0.842
Band 8A: Narrow NIR	20m	0.865

Band 9: water vapour	60m	0.945
Band 11: Cirrus	60m	1.1375
Band 11: SWIR 1	20m	1.61
Band 12: WRIR 2	20m	2.19

2.2. Method

Numerous remote sensing approaches and strategies have been established for mapping, monitoring, and assessing desertification. In the different zones (arid, semi-arid and sub-humid) affected by the phenomenon. In this paper, we rely on the extraction of several spectral indices such as NDVI, albedo, TGSi and MSAVI, and TCTs such as TCB, TCG and TCW. The approach adopted (Figure 2) is based on several steps, starting with the acquisition of sentinel-2A satellite images, data preprocessing where we performed an atmospheric correction, calculation of spectral indices (NDVI, albedo, TGSi, and MSAVI) and TCTs (TCB, TCG, TCW). Analysis of linear correlation between indices to select the best inverse correlation. Development and application of an indicator to extract the different desertification degrees in our region. Field surveys and data from the National Forest Inventory (NFI) are used to validate the desertification sensitivity map.

A receiver operating characteristic (ROC) approach was used to evaluate the models' capacity to identify and validate the areas at risk of desertification.

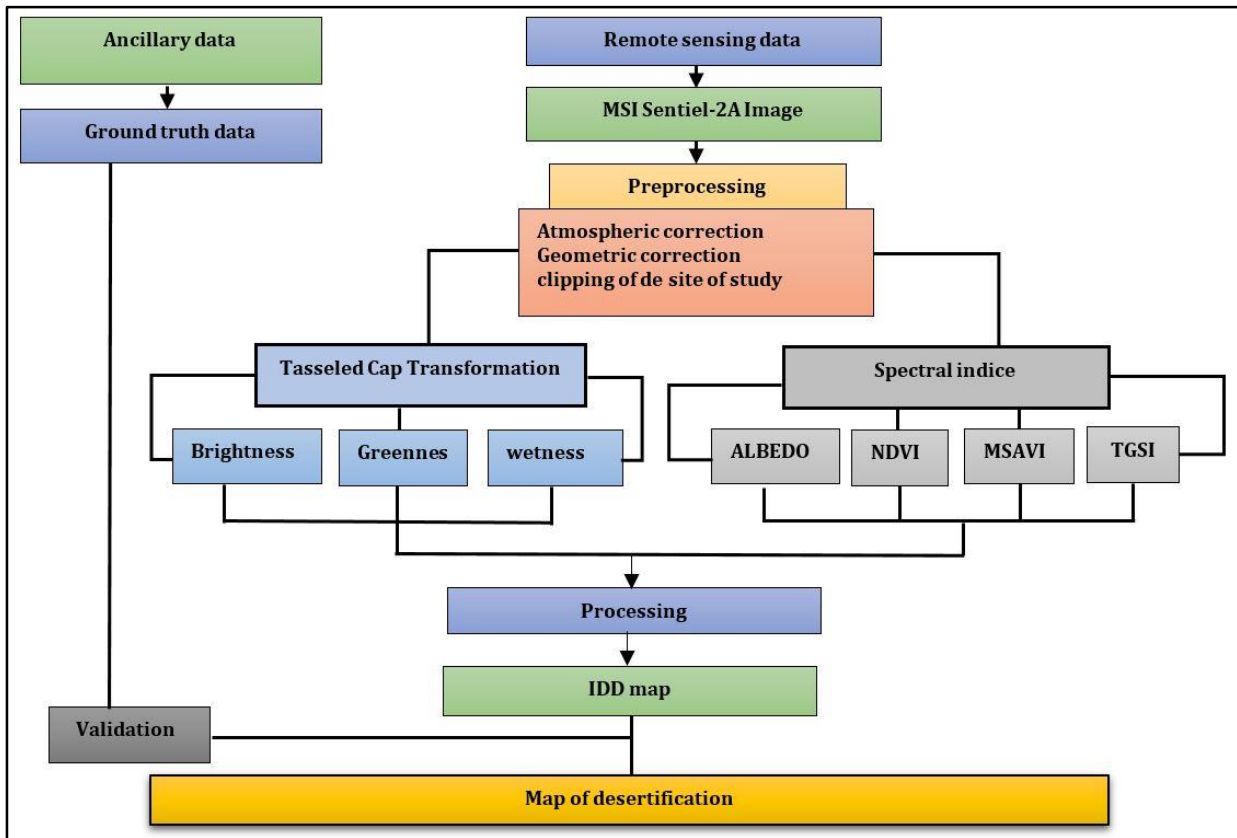


Figure 2. Methodologic flowchart

2.3. Satellite image preprocessing

As part of the Copernicus program, the European Space Agency developed the Sentinel-2 family (2A, 2B) of Earth monitoring satellites; the first two were launched in 2015 and 2017 [24, 27]. The Sentinel-2A satellites provide high-resolution multispectral images to continue the collection of data carried out by the Landsat and Spot missions while improving their quality [15].

This work was able to estimate the level of desertification within the Admer-Ezem sub-basin using a single image covering the basin. This cloud-free image was taken during the dry season (August 14, 2023). This

level 1 C image underwent geometric and radiometric correction to remove all distortions kinds in the images created by the sensor [15, 27-45] and atmospheric correction to remove the inaccuracy brought on by radiation from the atmosphere. The Sen2cor atmospheric correction toolbox is used to do this process, which is an algorithm integrated into the Sentinel Application Platform (SNAP) tool version 5.0 [46].

2.4. Derivation of spectral indices

Table 2. Formula and description of indices

Indices	Formulas	advantages	Authors
NDVI: Normalized difference vegetation index	$= (NIR - R) / (NIR + R)$	<ul style="list-style-type: none"> - Responsive to vegetation strength and abundance - Ability to assess plant health 	[47], [48], [49]
Albedo	$= ((0.356 - b2) + (0.130 - b4) + (0.373 - b8) + (0.085 - b11) + (0.072 - b12) - 0.018) / 1.016$	<ul style="list-style-type: none"> - Highlights moisture and soil content - Ideal for vegetation analysis - informs land cover and vegetation changes - improves classification accuracy 	[15], [50], [51]
MSAVI: modified soil adjusted vegetation index	$= (2 \times NIR + 1 - \sqrt{((2 \times NIR + 1)^2 - 8(NIR - RED))}) / 2$	<ul style="list-style-type: none"> - Allows vegetation to be characterized by taking into account soil humidity. 	[5], [52], [53]
TGSI: Topsoil Grain Size Index	$= (RED - BLUE) / (RED + BLUE + GREEN)$	<ul style="list-style-type: none"> - Refers to the classification and measurement of the proportions of sand, silt and clay in the topsoil. 	[54], [55], [56]

TCT Tasseled cap Transformation	TCB brightness	$= 0.3037 * B02 + 0.2793 * B03 + 0.4743 * B04 + 0.5585 * B08 + 0.5082 * B10 + 0.1863 * B12$	- Identification of changes in vegetation, soil and other characteristics resulting from human action.	[24] - [27] - [57]
	TCG greenness	$= -0.2848 * B02 - 0.2435 * B03 - 0.5436 * B04 + 0.7243 * B08 + 0.0840 * B11 - 0.1800 * B12$		
	TCW wetness	$= 0.1509 * B02 + 0.1973 * B03 + 0.3279 * B04 + 0.3406 * B08 - 0.7112 * B11 - 0.4572 * B12$		

The five indicators' relation was examined using the Pearson test (Albedo, NDVI, TGSi, MSAVI, TCB, TCG and TCW) (table 2). With "x" as the independent variable and "y" as the dependent variable, linear regression analysis may be carried out using the equation $y=ax + b$ in a characteristic space. We used albedo, TGSi and TCB as independent variables and NDVI, MSAVI, TCG and TCW as dependent variables for the combinations made.

To demonstrate the links between each of the two variables, we organized a random sampling, 199 points in the entire study area except irrigated areas, each point takes five values, the latter representing the pixels values of each band (NDVI, Albedo, TGSi, MSAVI, TCB, TCG and TCW).

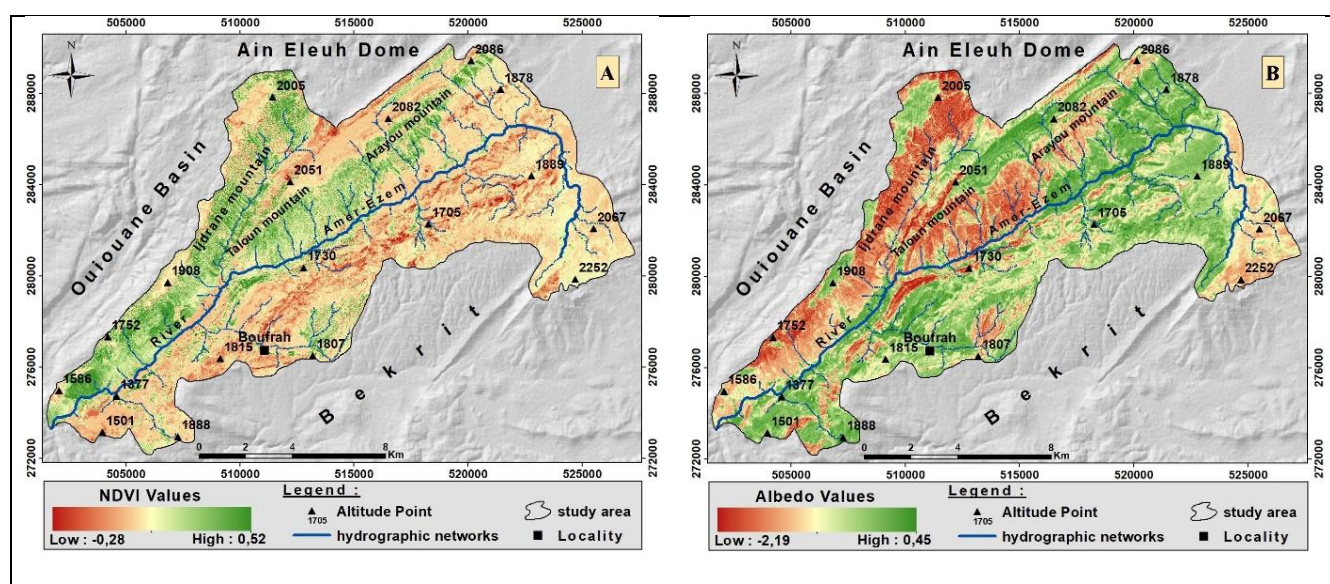
Based on the correlation rate, three combinations were used: (i) Albedo-TGSi, (ii) TGSi-TCW, (iii) TCW-TCB, as they give a better inverse correlation for calculating the IDD.

3. Results

3.1. TCT, NDVI, Albedo, MSAVI and TGSi

Figure (3) shows the results obtained from four spectral indices (Albedo, NDVI, MSAVI and TGSi) and the TCT indices (TCB, TCG and TCW). The highest values of NDVI and MSAVI and TCG (Figure 3a, d, f) correspond to the areas of dense vegetation cover particularly at the

level of the mountains of Jbel Taloune, Arayou, Ijdrane, as well as, to the irrigated fields along the Boufrach and Admer-Ezem wadi. On the other hand, the small values (-0.28 and -0.22 respectively) correspond to the bare soils generally found in the center of the basin and along the banks of the Admer-ezem wadi, particularly on the left bank. For albedo, the values vary between -2.1 and 0.45 (Figure 3b). High albedo values represent areas with low vegetation and bare and clear soil, while low values represent dense vegetation, especially at Jbel Taloune, Arayou, Ijdrane. For the TCB index (Figure 3e), the values varying between 0.24 and 1.37; and high albedo and TCB values indicate clear soils with a whitish color. The TGSi index gives details on the granulometry of the topsoil [15], this index values range between -0.82 and 0.74, the highest values, which are precisely in the center of the basin under study, show a coarse granulometry of the topsoil and, as a result, a high sand content and more degraded regions (Figure 3c). Soil moisture is measured by the TCW indice (Figure 3g), which has values ranging from -0.30 to 0.07. Wetlands, water bodies, and thick vegetation are associated with high TCW values, while barren soils with no vegetation cover are represented by low values.



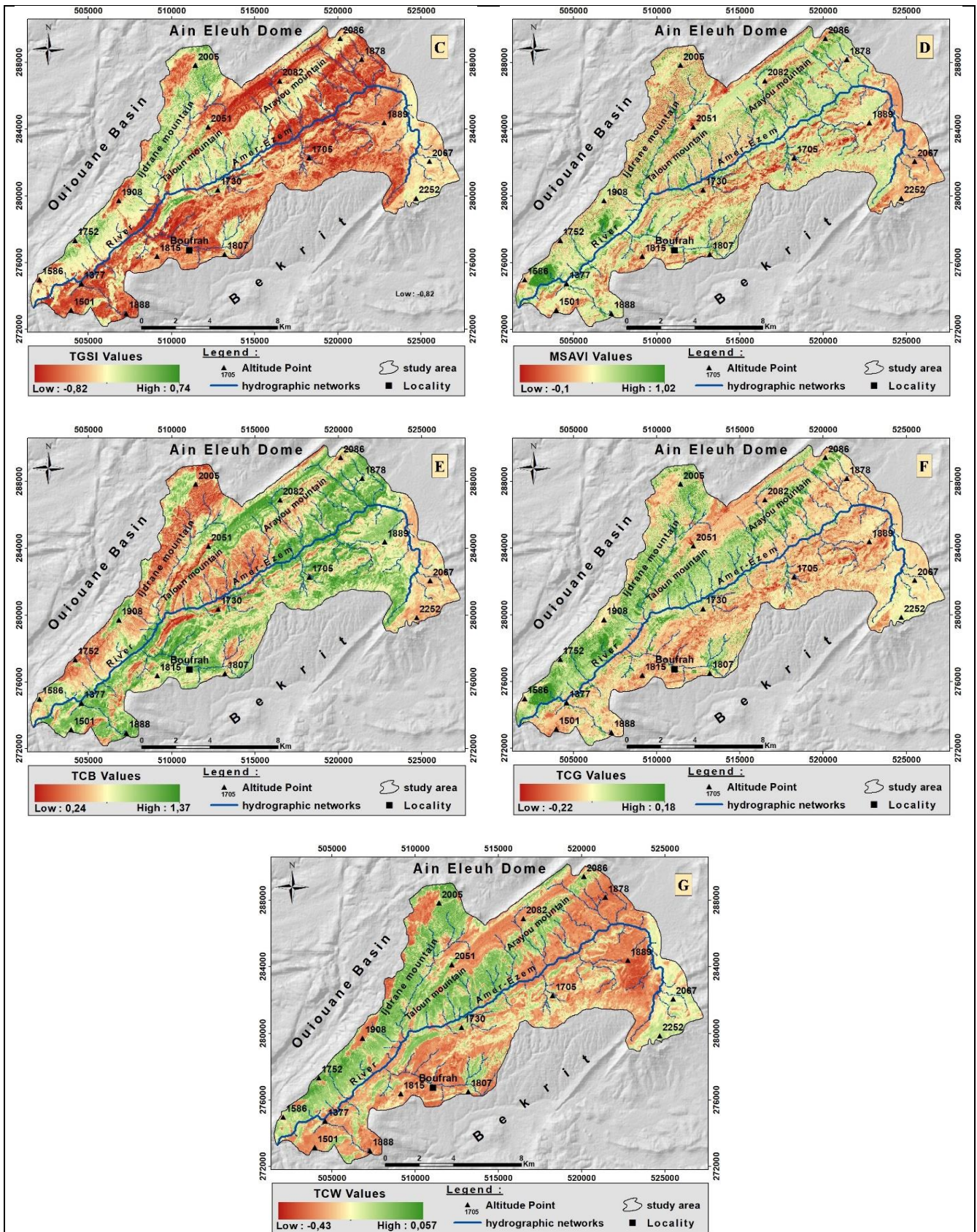


Figure 3. The four obtained indices; A: NDVI, b: Albedo, C: TGSi and D: MSAVi, and the three indices TCT E: Tasselled Cap brightness; F: Tasselled Cap greenness and G: Tasselled Cap wetness map

3.2. Linear Regression Analysis

Finding the best combination that has a very negative correlation and offers a very clear visual depiction of the various land cover types is the primary goal of linear correlation [24, 27]. There is a significant negative connection between TGSi and Albedo ($R=-0.95$) (Figure 4a) and between TGSi and TCW ($R=-0.74$) (Figure 4b),

according to results of linear regression analysis for the three sets. This suggests that as TCW and Albedo rise, TGSi falls, suggesting little to no desertification, and vice versa. TGSi rises as TCW and Albedo fall, suggesting that desertification is affecting the region. Additionally, the association between TCB and TCW is more negative ($R=-0.73$) (Figure 4c). This finding shows that while the TCB

risers as the desertification process intensifies, the TCW progressively falls (Figure 6). Three 2D feature spaces were generated for the whole region (Figure 5) based on

the layers of these seven indices, and they were compared to the three graphs that had already been made (Figure 4).

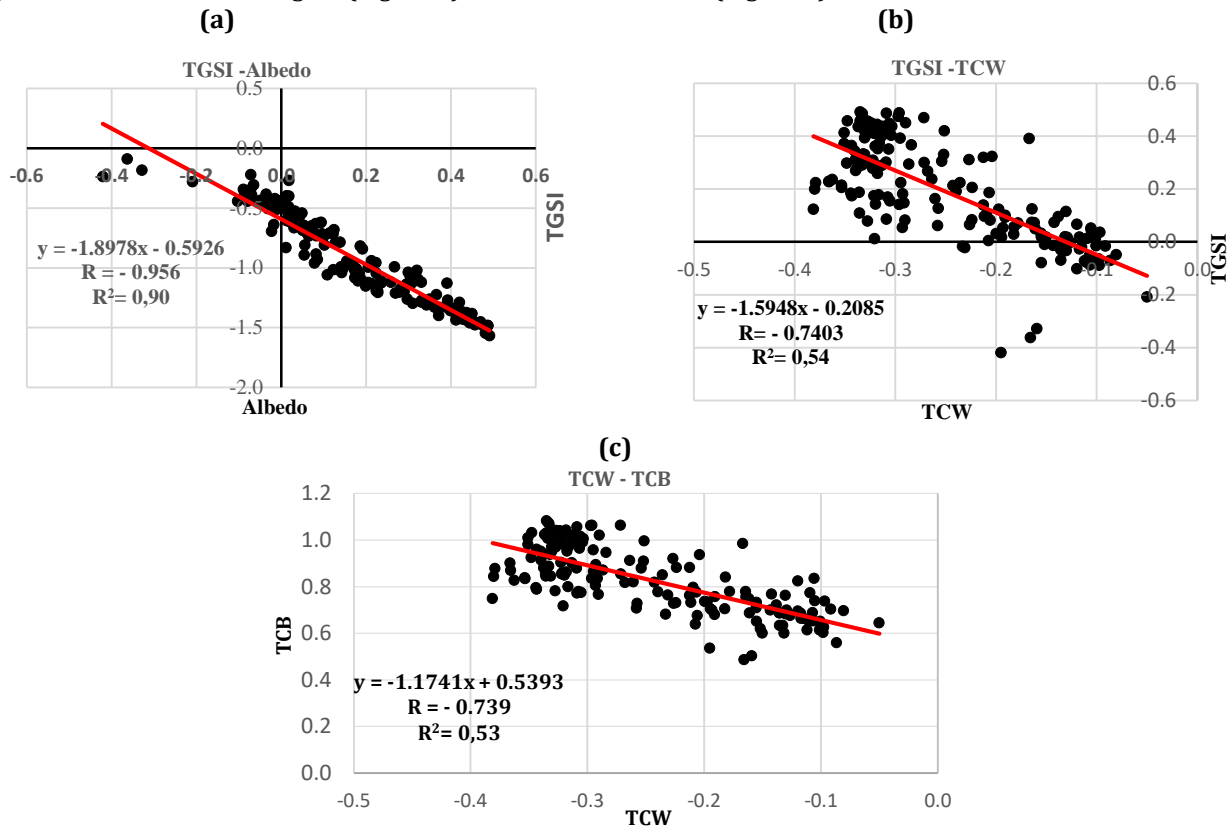


Figure 4. Linear correlations of the 3 combinations for 2021

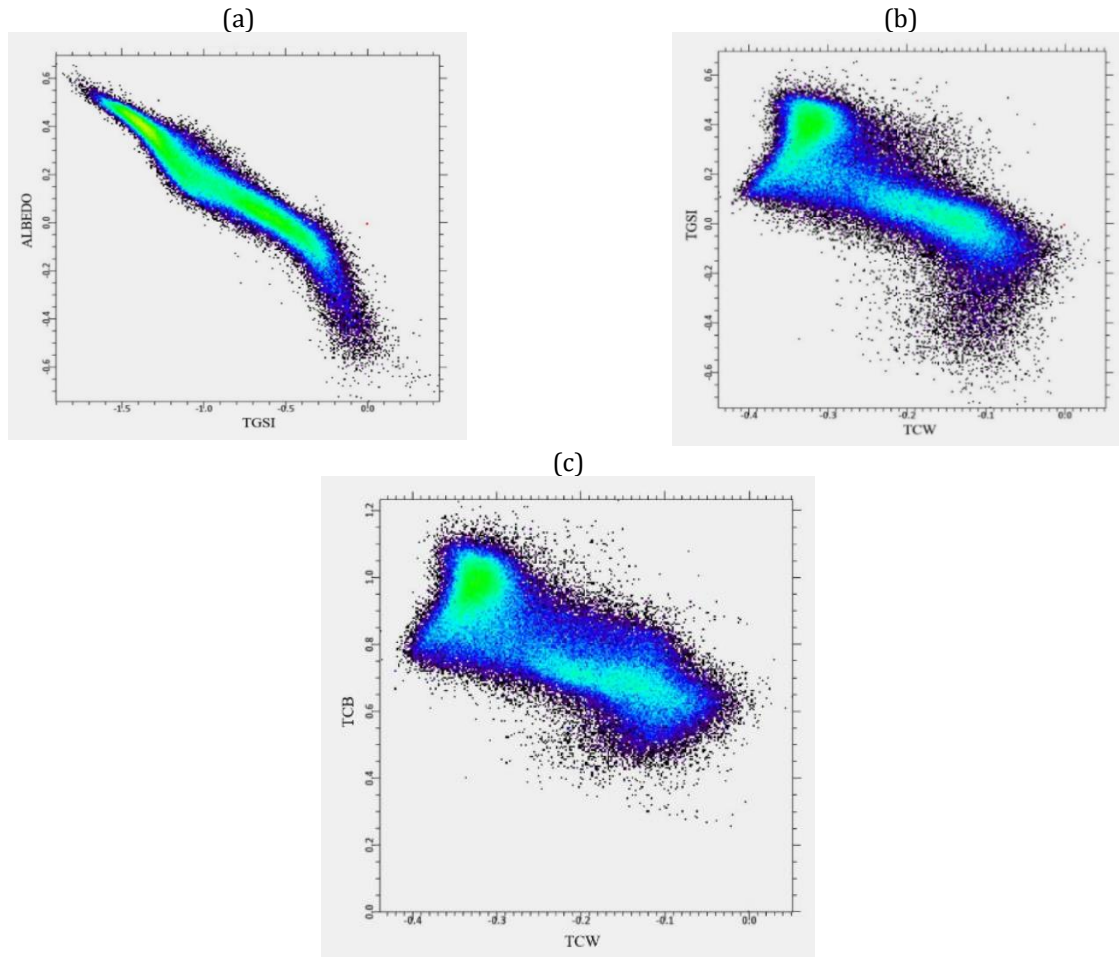


Figure 5. Scatterplot diagrams of: a) Albedo-TGSi, b) TGSi-TCW and c) TCB-TCW combinations.

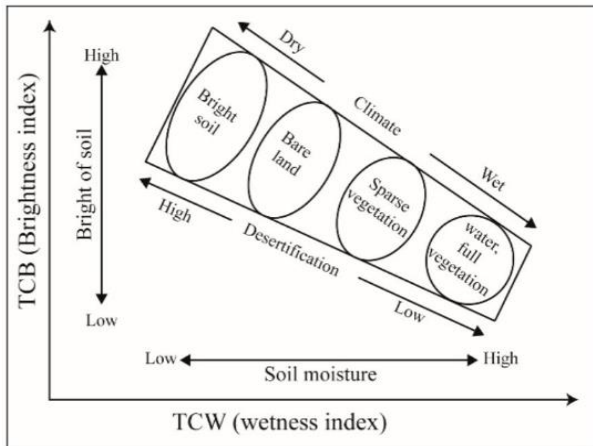


Figure 6. Desertification degrees in relation with soil greenness (TCG) and wetness (TCW) indicators

3.3. Results and the desertification degrees index (DDI) comparison

According to [15, 35-50], the desertification degree index is the best model for verifying an excellent mapping with high precision of the fragility to desertification in arid and semi-arid areas. The geographical classification of created combinations serves as the foundation for this approach.

The three feature space models represents the “DDI”, and α is the slope of the fitted straight line in each combination (Table 3). The Jenks natural break procedure is then used to classify the determined desertification degree values into five groups [57-58].

Many researchers have found success with this approach to categorize the occurrence of desertification in arid and semi-arid areas [24, 35, 50-59].

Consequently, the following formulae may be used to determine the DDI (7 and 8 and 9):

$$DDI(TCB-TCW) = \alpha (TCB - TCW) \quad (7)$$

$$DDI(TGSI-TCW) = \alpha (TGSI - TCW) \quad (8)$$

$$DDI(TGSI-Albedo) = \alpha (Albedo - TGSI) \quad (9)$$

Table 3. (a) Values for the three combinations

The combinations (models)	(a) values
(TCB-TCW)	-0,85
(TGSI-TCW)	-0,62
(TGSI-Albedo)	-0,52

The objective of the data clustering technique is to identify the optimal distribution of values among several classes [15, 35]. Thus, the five desertification categories obtained by using the “Jenks’ natural break” classification [58], are; extreme, severe, moderate, low and no-desertification. The table above shows these several categories jointly with the appropriate DDI values (Table 3).

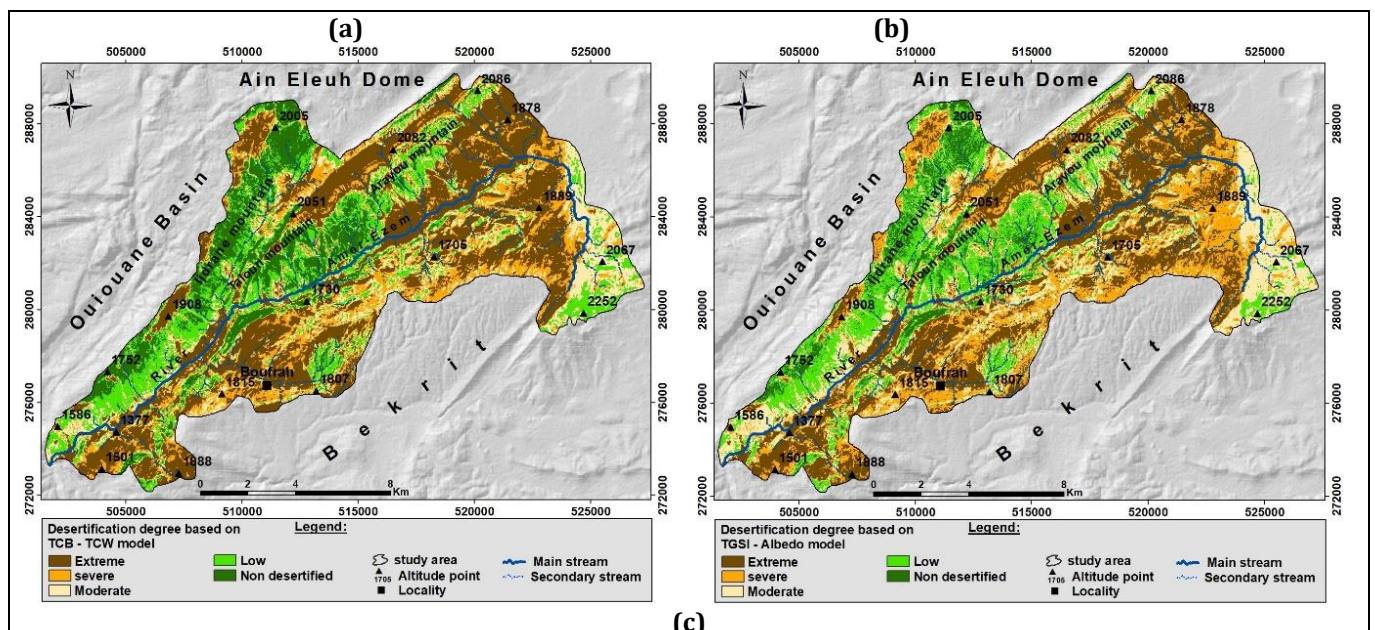
Table 4. An overview of the DDI values and desertification categories.

Desertification categories	TCB-TCW	TGSI- Albedo	TGSI-TCW
No-desertification	$DDI \geq 0,83$	$DDI \geq 0,79$	$DDI \geq 0,37$
Low	$0,83 < DDI \leq 0,71$	$0,79 < DDI \leq 0,55$	$0,37 < DDI \leq 0,24$
Moderate	$0,71 < DDI \leq 0,60$	$0,55 < DDI \leq 0,32$	$0,24 < DDI \leq 0,11$
Severe	$0,60 < DDI \leq 0,48$	$0,32 < DDI \leq 0,09$	$0,11 < DDI \leq -0,02$
Extreme	$DDI \leq 0,48$	$DDI \leq 0,09$	$DDI \leq -0,02$

3.4. Desertification Mapping:

Table (4) presents the results of the IDD calculations according to the three used models: TCB-TCW and TGSI-Albedo and TGSI-TCW.

According to the results obtained by the TCB-TCW model (Figure 7a); more than 68% of the Admer-Ezem basin is affected by desertification, of which 15.64% (30.94 km²) is classified as moderate, 18.15% (35.85 km²) as severe, and 35.01% (69.24 km²) as extreme. Non-desertified and slightly affected areas represent 12.91% (25.54 km²) and 18.29% (36.17 km²) of the study area, respectively.



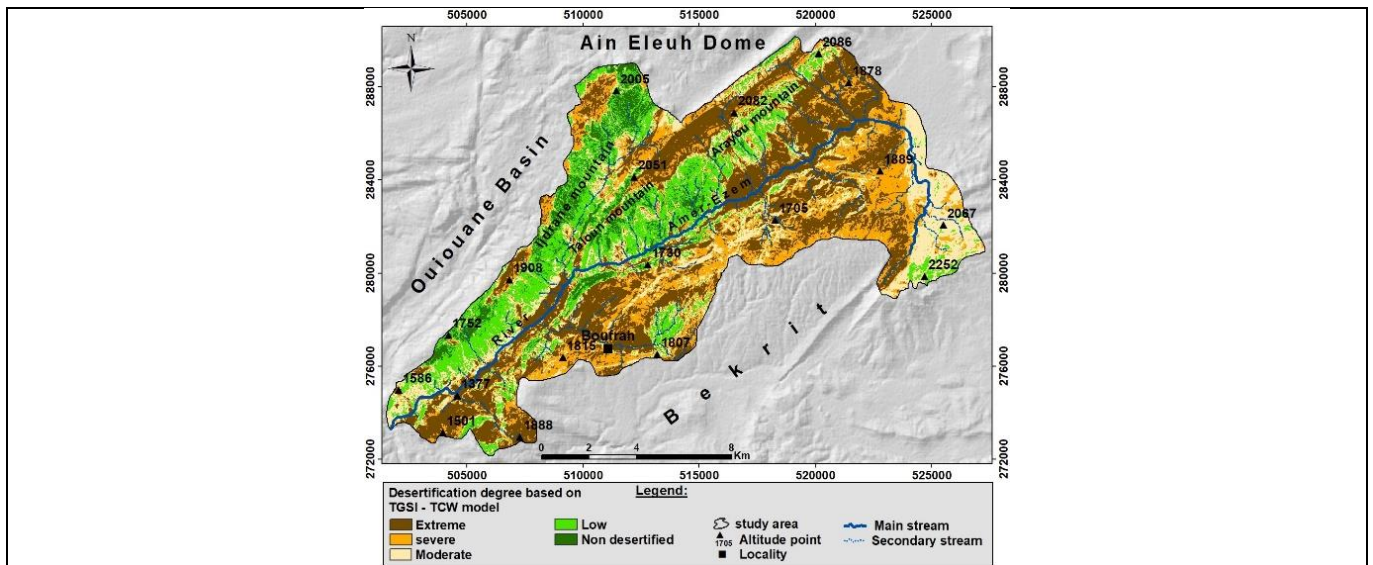


Figure 7. Maps of the state of desertification in basin of Admer-Ezem 2023; a: TCB-TCW, b: TGSi- Albedo et c: TGSi-TCW

The TGSi-Albedo model (Figure 7b) shows that 74.99% of the Admer-Ezem basin is affected by desertification, of which 21.74% (43 km²) is moderately desertified, 23.54% (46.5 km²) for severe desertification, and 29.71% (58.76 km²) for extreme desertification. Areas with low desertification and no desertification represent 18.68% (36.95 km²) and 6.33% (12.53 km²) of the total area of the Admer-Ezem basin, respectively. Finally, the TGSi-TCW model (Figure 7c) shows that 74.71% of the Admer-Ezem basin is threatened by moderate to extreme desertification, including 20.1% (39.76 km²) for moderate desertification, 22.04% for severe desertification (43.59 km²), and 32.57% (64.45 km²) for extreme desertification. Areas with low desertification and no desertification represent 19.42% (38.38 km²) and 5.85% (11.58 km²) of the study area, respectively. The results obtained by the three models are almost identical,

Table 5. Statistical analysis of the extraction of information on desertification by TCB-TCW, TGSi- Albedo and TGSi-TCW.

Desertification categories	TCB-TCW		TGSi- Albedo		TGSi-TCW	
	Area (km ²)	%	Area (km ²)	%	Area (km ²)	%
Non-desertification	25,54	12,91	12,53	6,33	11,58	5,85
Low	36,17	18,29	36,95	18,68	38,38	19,42
Moderate	30,94	15,64	43	21,74	39,76	20,1
Severe	35,85	18,15	46,5	23,54	43,59	22,04
Extreme	69,24	35,01	58,76	29,71	64,45	32,57
Total	197,74	100	197,74	100	197,74	100

3.5. Evaluation and comparison of desertification map accuracy

For a good evaluation of the land susceptibility maps to desertification, a sampling of 199 points was collected with the photos and attributes of each point. During many field excursions conducted in March and July 2024, the ground truth points were gathered from various desertification classes (complete vegetation cover, moderate vegetation cover, sparse vegetation, light soil, dark soil, and water). In conclusion, the sample's homogeneity and accessibility were taken into consideration while choosing the points.

To evaluate the ability of the models to assess the areas sensitive to desertification risk and validate its

with a slight difference between the surface area of each category (Table 5; Figure 8). Severe and extreme desertification areas are most dominant in the Admer-Ezem basin. The majority of them are located on the eastern slopes of the N-Tifratine-Arayou Arhoun mountain range, also on the southern and south-eastern slopes, mainly areas with steep slopes that suffer from poor plant cover and successive anthropogenic pressure, mainly agriculture in Bour and pastoralism on the northern slopes of Jbel Elkoubate. The areas with low desertification are located in the areas characterized by a less dense vegetation cover, and also at the level of the irrigated perimeters along the Admer-Ezem basin, and its tributary Oued Boufrah and its tributarie. The desertified areas, they are located in the peaks of the Aryou, Ijdrane, Ahroun mountains, where the density of the vegetation cover and the weakness of the slope and the absence of the anthropogenic impact.

sensitivity, a receiver operating characteristic (ROC)

approach was used (Figure 7). [24, 60, 56 - 61] have identified five categories for the AUC score: bad (0.5-0.6), average (0.6-0.7), good (0.7-0.8), very good (0.8-0.9), and perfect (0.9 1.0).

The following results indicate that the three models are very adequate to delineate areas at risk of desertification, with an accuracy of 83% for the TCB – TCW model, 82% for TGSi -TCW and 78% for the TGSi – Albedo model (Figure 7).

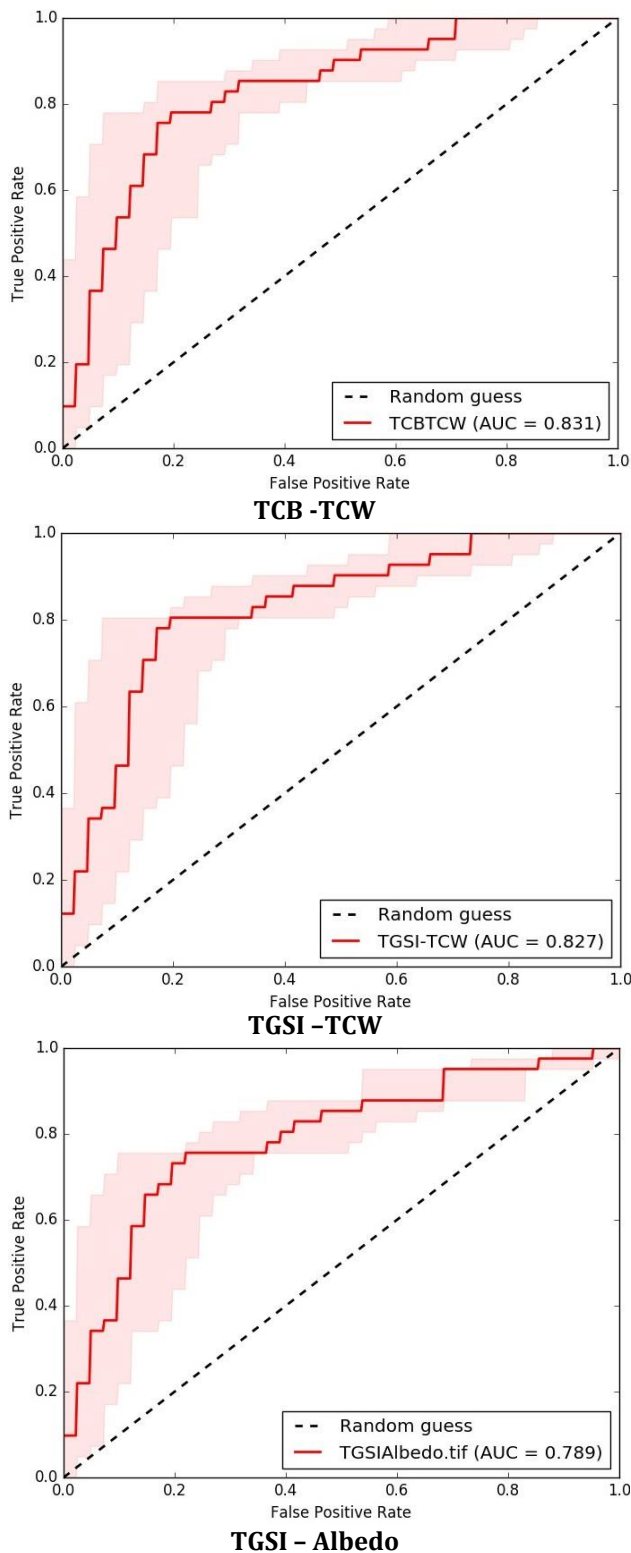


Figure 8. ROC curve of the DDI model validation in Amer-Ezem basin

4. Discussion:

Desertification poses a major danger to the social economy and ecology, which is a research area for many researchers in various arid and semi-arid areas affected by this phenomenon, particularly in Middle East, Asia and North Africa, which are characterized by a high risk of desertification. Several techniques and methods have been used worldwide for the assessment and mapping of desertification. These methods vary in complexity from basic to advanced, which are mainly based on different indices, such as the studies made by several authors in

Brésil namely the research of [62] on the use of "RisDes" Index to analyze the advancement of areas undergoing desertification using satellite data. The results obtained from this "RisDes" index showed that the area of desertified zones increased by 34% between 1991 and 2016 in the region (Cabrobó DN).

[63] Who analyzed the desertification of grasslands due to coal mining from remote sensing in Huolinhe (china), he concluded that the severe desertification area of grassland is increasing in the past 16 years, and there is a strong correlation between mining land and the severe desertification area of grassland. According to the characteristics of grassland desertification in open-pit coal mine. Other studies highlight this phenomenon such as that of [12] on land desertification and its influencing factors in Kazakhstan, and the investigation of [35] on the integration of remote sensing techniques for desertification monitoring in Mexico, which shows that almost 16.4% of the territory is classified as severe to extreme. Other results from Iraq support our conclusions, including the research conducted by [5] based on the assessment of the degree of desertification by TCT and spectral indices, in a semi-arid space in Iraq. The results concluded that this area is very sensitive to desertification, while almost 45.67% of the general area is classified as severe to extreme. While the studies carried out in Africa, especially in Algeria, we cite the work of [64] who tried to map the land vulnerability to desertification using a logistic regression analysis in the Algerian Djelfa region; they concluded that approximately 44.57% of the studied area is classified as very vulnerable to desertification. [65] who monitored the phenomenon of desertification in northern Algeria concluded that approximately 75% of steppe rangelands are desertified or on the verge of desertification, also the work of [66] on mapping areas potentially subject to desertification in northeastern Algeria using a logistic regression model, GIS and remote sensing techniques. It's concluded that the results obtained show that the high and very high classes occupied 19.33% and 58.72% of the total land area respectively.





In Morocco, mainly in arid and semi-arid areas, numerous studies have been conducted on the quantitative assessment of the degree of desertification using several methods such as: the MEDALUS method and methods based on the use of several typical spectral indices, namely NDVI, albedo, MSAVI, TGSI, and TCT. Among these studies is the work of [15], which, based on the assessment of desertification in the Moulouya region, concluded that 61% of the basin is exposed to extreme and severe desertification risk.

While [24] in their paper, which concerns the quantitative assessment of desertification in the middle Draa Valley, found that 26.92% and 32.85% of the land falls respectively into the severe and extreme categories of the general area. In addition, the results of [27] in a region neighboring our area on the modeling of the desertification phenomenon using Sentinel 2A images and TCT indices, it concluded that almost 40% of the forest area is classified as being in severe to intense desertification. Other researchers are using the MEDALUS approach to assess the land sensitivity to

desertification, such as; the outcomes of [7] in the Souss watershed, which suffers from aridity and anthropogenic pressure, it also concluded that almost 47% of the general area is sensitive to desertification. Moreover, the study of [23] in the Oued El Maleh watershed, the researchers concluded that 35% of the watershed is very sensitive to desertification. In addition, the [25] result's on the upper Oueghra in the northern Morocco concluded that the areas with very high sensitivity to desertification represent approximately 26.85% of the the basin studied. As for [67] in their research on the Middle Moulouya basin concluded that approximately 35.47% of this basin is exposed to a high risk to desertification. For [26] in their examination on the Ouergha watershed in northern Morocco concluded that more than half of the basin has an average sensitivity of land to degradation.

The results of TCB-TCW analysis show a strong negative correlation ($R = -0.73$), this is consistent with the results of [5, 24 -68] who concluded that TCW can be closely related to soil management and vegetation cover.

Table 6. Summary and description table of the different degrees of desertification in the Admer-Eem basin

	Field image	Description
Non-desertification		Located at the tops of the highest mountains: Taloun, T-N tifraine and Ijdrane, Ain Kahla dome where the forest is very dense, these areas are characterized by the definitive absence of degradation factors. And also, a very resistant substrate and a very low slope.
Low		These areas mainly refer to a moderate density dominated by a mixture of cover that includes holm oak and some junipers. These areas are used in pastoralism and firewood needs.
Moderate		Located on the southern and southeastern slopes of the east are dominated by this type of scrubland, these areas are very sensitive to the phenomenon of desertification, they require intervention to balance the environment and human activities.
Severe		Located in the middle of the basin and on the northern slope of T-N-Tifratine also at the level of the eastern slopes of Jbel elkoubate, these areas are characterized by the dominance of degraded scrubland and degraded pastures, human activity is very intense, and the human-environment balance is very broken.

While the TGSI-Albedo model perfectly reveals the extreme contrast between the top soil layer and land surface albedo. The results of TGSI-Albedo analysis show a strong negative correlation ($R = -0.95$), this rate is almost similar with the results of [69] who concluded that TGSI could be strongly related to selection as an indicator of reaction to surface conditions of plant biomass. In addition, the TGSI-TCW model undoubtedly highlights the clear difference between the upper soil layer and dry soils. Subsequently, the results obtained from the TGSI-TCW model show a strong negative correlation ($R = -0.74$). In the absence of any study on desertification at the scale of Admer-Ezem, we carried out a comparison between the results of the three models and the reality based on field visits as well as the use of high-resolution satellite images using the ROC technique (table. 6). This task seems necessary to confirm the results of the desertification state in the studied area, the correlation results were very precise ($AUC_{(TCB-TCW)} = 83\%$; $AUC_{(TGSI-TCW)} = 82\%$; $AUC_{(TGSI-Albedo)} = 78\%$).



Located in the central part of the basin and in the eastern slopes of the N-Tifratine, Taloun, Ahroun mountain range overlooking the Admer-Ezem valley. It affects the entire basin at different scales and reflects the lack of vegetation cover and poor land management. (These areas are characterized by the presence of different forms of erosion).

4.1. Desertification factors:

Among the causes of the increasing severity of the desertification phenomenon, they are summarized in natural causes linked to climatic conditions. Indeed, the succession of drought is the main characteristic of the Admer-Ezem basin. The analysis of climatic data shows

that the basin experienced a climate characterized by a large intra-annual and intra-monthly variability. According to the results of the standardized precipitation index (SPI), carried out from data from the Tamchachat station figure (9), the basin has experienced a succession of years of drought.

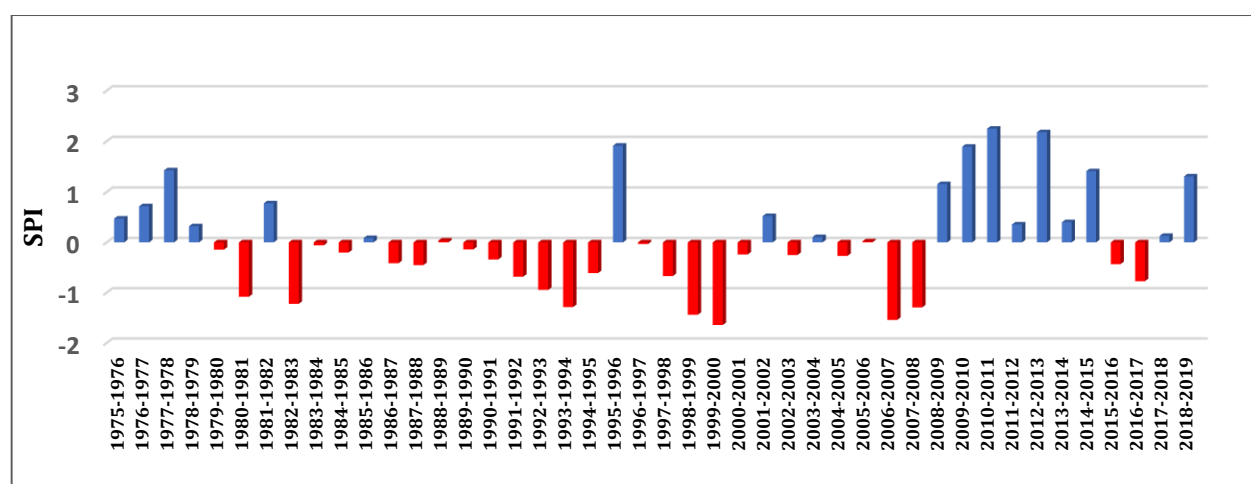


Figure 9. SPI during the period 1975–2020 in the station of Tamchachat.

High temperatures are another characteristic of the area that can reach 39 °C in July and August, which contributes to the increase in evapotranspiration that can reach 95 mm during the dry months (July and August). These climatic conditions contribute largely to the evolution of the desertification phenomenon (Figure 8).

As for the second factor, it is assimilated to all human activities characterized by overexploitation of land. Since independence, the basin has experienced a sedentarization of the local population along the wadis, which already knew a nomadic pastoral life, to integrate

pastoralism and irrigated agriculture as an economic source of survival. This population has also experienced significant demographic growth, since the population of different douars composed of the study area increased from 1247 habitants in 1982 to 1259 in 1994, to 2826 inhabitants in 2004, to 3088 inhabitants in 2014 with a growth rate of 1.6%. This demographic evolution exerts great pressure on natural resources (vegetation cover and soil). The overexploitation of these resources manifests itself in several forms, namely the excessive collection of firewood, overgrazing and plowing of steep slopes (Figure 9).





Figure 10. Manifestations of human pressure: (a) Anthropogenic pressure on slopes (plowing) (b) wood cut down by the Water and Forests Agency, (c) wood oriented towards exploitation in houses, (d) random deforestation

4.2. Limitations and difficulties

Assessing desertification using a combination of TCT spectral indices, GIS, and remote sensing is a useful tool for evaluating environmental risks, but it has several drawbacks. Spectral indices such as NDVI, MSAVI, Albedo... mainly reflect the condition of the soil or vegetation, but do not directly reflect the complexity of degradation processes such as erosion, salinization, or loss of fertility. Furthermore, these indicators are sensitive to seasonality and atmospheric conditions, and can be a source of misunderstanding, for example between areas that are actually degraded and light-colored soils. The used satellite images suffer from significant limitations, such as the low spatial resolution of Sentinel-2A data (10 to 30 m), which makes it impossible to detect local microprocessors or fine degradations. Their temporal resolution and the frequent occurrence of nuages are other limitations [70-72]. In addition, there are uncertainties associated with radiometric adjustments, scale variances, and heterogeneity of the data included in the SIG. On a methodological level, the analysis of indicators and the development of models frequently rely on subjective or empirical decisions, which may affect the reliability of the findings.

5. Conclusion:

In this study, we developed three models (TGSI-Albedo, TGSI-TCW, TCW-TCB) to assess the desertification risk in the Admer-Ezem basin using Sentinel-2A images.

It was noted that the three models, TCW-TCB and TGSI-Albedo and TGSI-TCW, presented a good result in assessing the degree of desertification with an overall accuracy of AUC = 83.1% and 78.9% and 82.7% respectively.

The results obtained from the use of the three models show that non-desertified areas represent 5% to 15% of the basin, low-risk areas between 18% and 19.5%, medium-risk environments between 15% and 22%, severe-risk areas between 18% and 23.5%, while extreme-risk areas represent 29% to 35% of the study area. Validation of the results of the three models (TGSI – Albedo, TGSI -TCW, TCB -TCW) gives good scores

ranging from 78% to 83%, with a preference for the last model.

The results obtained represent a useful tool for different stakeholders. Engineers, planners and authorities to effectively combat desertification. Based on the results, the methodology adopted in this article remains sufficiently effective to extend desertification risk maps to other similar Moroccan mountainous regions and can be transferable to other arid and semi-arid regions, particularly in North Africa, the Middle East and Asia. This model can assist planners in determining the best locations for future forest development.

Acknowledgement

The authors express their gratitude to all individuals and institutions that provided support and resources for this research.

Author contributions

Abdelhak Limame contributed to the conceptualization, data collection, satellite imagery processing, analysis, manuscript editing, critical review and manuscript writing. **Khalid El Hairchi** was responsible for supervision, critical review, manuscript editing and granted final approval for manuscript submission.

Lahcen Ouiaboub was responsible for analysis and critical review.

Conflicts of interest

The authors declare no conflicts of interest.

References:

1. Imeson, AC. (1996). Desertification research—Thematic issues and spatial and temporal scaling. In: Hill J, Peter D (eds) The use of remote sensing for land degradation and desertification monitoring in the Mediterranean basin. European Commission, Brussels. <https://hdl.handle.net/11245/1.125472>
2. Rubio, J.L., & Recatala, L. (2006). The relevance and consequences of Mediterranean desertification including security aspects. In: Kepner WG, Rubio JL, Mouat DA, Pedrazzini F (eds) Desertification in the Mediterranean Region: a security issue. Springer, Netherlands,

- pp. 133–165. [https://doi :10.1007/1-4020-3760-0_05](https://doi.org/10.1007/1-4020-3760-0_05)
3. Duanyang, X., Xiangwu ,K., Dongsheng, Q., Dafang, Z., & Jianjun, P.(2009). Quantitative Assessment of Desertification Using Landsat Data on a Regional Scale – A Case Study in the Ordos Plateau, China. *Remote Sensors* (Basel). 2009, 9(3),pp. 1738-1753. <https://www.ncbi.nlm.nih.gov/pmc/articles/PMC3345839/#>.
 4. Guo, Q., Fu, B., Shi, P., Cudahy, T., Zhang, J., & Xu, H. (2017). Satellite Monitoring the Spatial-Temporal Dynamics of Desertification in Response to Climate Change and Human Activities across the Ordos Plateau, China. *Remote Sens.*, 9, 525. [CrossRef].
 5. Reem Tuama, Y., & AL-khakani, E.T. (2021). Assessing Degree of Desertification Using Tasseled Cap Transformation and Spectral Indicators Techniques: Iraq. *The Scientific Journal of King Faisal University*, Volume (2).Issue (1). <https://doi.org/10.37575/b/sci/0019>
 6. UNCCD (1994). United Nations Convention to Combat Desertification in those Countries Experiencing Serious Drought and/or Desertification, particularly in Africa; United Nations Convention to Combat Desertification: United Nations Paris, France., Treaty Series, vol. 1954, p. 3. [Google Scholar]
 7. Bouabid, R., Rouchdi, M., Badraoui, M., & Louafi, S. (2010). Assessment of land desertification based on the MEDALUS approach and elaboration of an action plan: the case study of the Souss River Basin, Morocco. *Land degradation and desertification: assessment, mitigation and remediation*. Springer, pp 131–145. <https://www.researchgate.net/publication/251100743>
 8. Ekundayo, A., Oluibukun, A., Joseph, O., & Abel, I. (2024). Assessing the risk of soil loss using geographical information system (GIS) and the revised universal soil loss equation (RUSLE). *Advanced GIS*. 4(2),pp. 42-53. <http://publish.mersin.edu.tr/index.php/agis/index- ISSN:2822-7026>.
 9. Thomas, D. S. G. (1995). Desertification: Causes and processes, In: *Encyclopedia of Environmental Biololgy*, Vol. 1, ed. W. A. Nierenberg, San Diego, Academic Press,pp. 463-473. [Google Scholar]
 10. Array, A. (1989). Current Issues and Trends in Irrigation with Special Reference to Developing Countries, In: "Resource Conservation and Desertification Control in the Near East, Report of the International Training Course, DSE, FAO, GTZ, UNESCWA, Germany and Kingdom of Jordan.
 11. Verbist, K., Santibañez, F., Gabriels, D., & Soto, G. (2010). Atlas de zonas áridas de América Latina y El Caribe. : dentro del marco del proyecto elaboración del Mapa de Zonas áridas, Semiáridas y Subhúmedas de América Latina y el Caribe. http://www.cazalac.org/mapa_zs.php
 12. Hu, Y., Han, Y., & Zhang, Y. (2020). Land desertification and its influencing factors in Kazakhstan. *J Arid Environ* 18+0:104203. <http://dx.doi.org/10.1016/j.jaridenv.2020.104203>
 13. Khorrami, B., Gunduz, O., Patel, N., & Ghouzlane, S. (2019). Land surface temperature anomalies in response to changes in forest cover. *International Journal of Engineering and Geosciences*, 4(3), pp. 149-156. <https://doi.org/10.26833/ijeg.549944>
 14. Herrmann, S., Diouf. A. A., & Sall, I. (2020). Beyond bioproductivity: engaging local perspectives in land degradation monitoring and assessment. *J Arid Environ* 173:104002, <http://dx.doi.org/10.1016/j.jaridenv.2019.104002>
 15. Lamaamri, M., Lghabi, N., Ghazi, A., El Harchaoui, N., Adnan, MSG., & Shakiul Islam, M. (2022). Evaluation of desertification in the Middle Moulouya Basin (North-East Morocco) using sentinel-2 images and spectral index techniques. *Earth Syst Environ* pp.1– 20. <https://doi.org/10.1007/S41748-022-00327-9>
 16. Reynolds, J., Maestre, F., Huber-Sannwald, E., Herrick, J., & Kemp, P. (2006). Aspectos socioeconómicos y biofísicos de la desertificación: . *Ecosistemas*, 14(3). <http://www.revistaecosistemas.net/articulo.asp?Id=131>
 17. L'organisation arabe pour le développement agricole (OADA) .(2002). Etude des Indicateurs de Suivi de la Désertification dans le Pays Arabes. United Nations, Treaty Series ,vol. 1954, p. 3. [Google Scholar]
 18. El- Bouhali, A., Amyay, M., & El Ouazani Ech-Chahdi, K. (2024). Changes in water surface area of the Middle Atlas-Morocco lakes: A response to climate and human effects. *International Journal of Engineering and Geosciences*, 9(2), pp. 221-232. <https://doi.org/10.26833/ijeg.1391957>
 19. Boutallaka, M., Miloud, T., El Mazi, M., Hmamouchi, M., & EL Hairchi, K. (2025). Assessment of current and future land sensitivity to degradation under climate change in the upstream Ouergha watershed (Morocco) using GIS and AHP method. *International Journal of Engineering and Geosciences*, 10(1), 46-58. <https://doi.org/10.26833/ijeg.1521350>
 20. Mokhtari, N .(2016). Etude de la dynamique de la désertification dans le bassin versant de la Moulouya en intégrant les données issues de la télédétection et les données socio-économiques, Maroc (Thèse de doctorat). Université de Liège, pp.326. <https://www.academia.edu/79606011>
 21. MADREF (Ministère de l'Agriculture du Développement Rural et des Eaux et Forêts). (2020). Programme national de lutte contre la désertification: Rapport principal.p.135.

- <http://www.unccd.int/actionprogrammes/afri-ca/national/2002/morocco-fre.pdf>. Cited 15 Apr 2009
22. Bengrich, M. (1988). La désertification dans le bassin de Guercif (Maroc oriental): étude de géographie physique. Thèse de doctorat université Avignon, France, pp 265. <http://www.secheresse.info/spip.php?article7744>
 23. Yağmur, N., Tanık, A., Tuzcu, A., ... Musaoğlu, N. (2020). Opportunities provided by remote sensing data for watershed management: example of Konya Closed Basin. *International Journal of Engineering and Geosciences*, 5(3), 120-129. <https://doi.org/10.26833/ijeg.638669>
 24. Al Kalbani, K., & Rahman, A. A. (2022). 3D city model for monitoring flash flood risks in Salalah, Oman. *International Journal of Engineering and Geosciences*, 7(1), 17-23. <https://doi.org/10.26833/ijeg.857971>
 25. Ech-Chahdi-Ouazani, K., Elbouhali, A., & Amyay, M. (2022). La cartographie et caractérisation de la sensibilité à la désertification dans le bassin versant du haut Ouergha (Rif central-Maroc) par l'approche MEDALUS. *Geomaghreb*. No. 16 (20). <https://revues.imist.ma/index.php/Geomaghreb/article/view/30776>
 26. Boutallaka, M., El Mazi, M., Ben-Brahim, Y., & Houari, A. (2023). Mapping the sensitivity of land degradation in the Ouergha catchment (Morocco) using the MEDALUS approach. *Eurasian Journal of Soil Science*. <https://doi.org/10.18393/ejss.1276119>
 27. El Hairchi, K., Benbrahim, Y., Ouiaboub, L., Limame, A., & Saadi, O., Nouayti, A. (2023). Desertification modeling in the Moroccan Middle Atlas using Sentinel-2A images and TCT indexes (case of the Ain Nokra Forest). *Modeling Earth Systems and Environment*. <https://doi.org/10.1007/s40808-023-01752-z>
 28. Benabderrahmane, M.C., & Chenchouni, H. (2010). Assessing Environmental Sensitivity Areas to Desertification in Eastern Algeria using Mediterranean Desertification and Land Use "MEDALUS" Model. *Int. J. of Sustainable Water & Environmental Systems* Volume 1, No. 1. 5-10. <https://d1wqtxts1xzle7.cloudfront.net/31932973/swes201001005010-libre>
 29. Huang, S., & Siegert, F. (2006). Land cover classification optimized to detect areas at risk of desertification in North China based on SPOT VEGETATION imagery. *J. Arid Environ*. 67, 308–327. [CrossRef]
 30. Guang, Y., Dong, C., Xinlin, H., Aihua, L., Mingjie, Y., & Xiaolong, L. (2017). Land use change characteristics affected by water saving practices in Manas River Basin, China using Landsat satellite images. *Int. J. Agric. Biol. Eng*. 2017, 10, pp. 123–133. [CrossRef]
 31. Wang, X., Hua, T., Lang, L., & Ma, W. (2017). Spatial differences of aeolian desertification responses to climate in arid Asia. *Glob. Planet. Chang.*, 148, pp.22–28. [CrossRef]
 32. Hostert, P., Roder, A., & Jarmer, T., & Udelhoven, T. (2001). The potential of remote sensing and GIS for desertification monitoring and assessment. *Ann Arid Zone* 40:103–140. <https://d1wqtxts1xzle7.cloudfront.net>
 33. Wang, T., Yan, CZ., Song, X., & Xie, JL. (2012). Monitoring recent trends in the area of aeolian desertified land using Landsat images in China's Xinjiang region. *ISPRS J Photogramm Remote Sens* 68:184–190. <https://doi.org/10.1016/j.isprsjprs.2012.01.001>
 34. Sayl, K.N., Sulaiman, SO., Kamel, A.H., Muhammad, NS., Abdullah, J., & AlAnsari, N. (2021). Minimizing the impacts of desertification in an arid region: a case study of the West Desert of Iraq. *Adv Civ Eng*. <https://doi.org/10.1155/2021/5580286>
 35. Becerril-Piña, R., Díaz-Delgado, C., Mastachi-Loza, CA., & González-Sosa, E. (2016). Integration of remote sensing techniques for monitoring desertification in Mexico. *Hum Ecol Risk Assess an Int J* 22:1323–1340. <https://www.researchgate.net/publication/299653857>
 36. Zeng, Y., Feng, Z., & Xiang, N. (2006). Albedo-NDVI space and remote sensing synthesis index models for desertification monitoring. *Sci Geogr Sin* 26:75. <https://doi.org/10.13249/j.cnki.sgs.2006.01.75>
 37. Guo, B., & Wang, F. (2020). Dynamic monitoring of desertification in Naiman Banner based on feature space models with typical surface parameters derived from LANDSAT images. *Land degradation & développement* Volume 31, Issue 12 pp 1573-1592. <https://doi.org/10.1002/ldr.3533>
 38. Wei, H., Wang, J., Cheng, K., Li, G., Ochir, A., Davaasuren, D., & Chonokhuu, S. (2018). Desertification information extraction based on feature space combinations on the Mongolian plateau. *Remote Sensing*, 10(10), 1614. <https://doi.org/10.3390/rs10101614>
 39. Limame, A., Hanchane, M., Zhar, M., El hairchi, K., & Lamaamri, M. (2022). Variabilité climatique et ses impacts sur le régime hydrologique de l'oued Améngous-Fellat, Haut bassin de l'Oum-Rbia (Maroc). *Acte de colloque Les risques hydroclimatiques et géomorphologiques : typologie, cartographie et gestion*. Oujda. Pp 41-46. <http://lettres.ump.ma/fr/actes-du-colloque-international-les-risques-hydroclimatiques-et-geomorphologiques-typologie-cartographie-et-gestion>
 40. Yilmaz H.M., Yakar M., Yildiz F., Karabork H., Kavurmaci M.M., Mutluoglu O., & Goktepe A. (2010). Determining rates of erosion of an earth pillar by terrestrial laser scanning. *Arab. J. Sci. Eng*. 35(2A), 163–172 (2010)

41. Lecompte, M. (1969). La végétation du Moyen Atlas central : esquisse phyto-écologique et carte des séries de végétation au 1/200000. R.G.M., pp. 3 - 34. Rabat.
42. Lecompte, M., & Lepoutre, B. (1975). Bilan de l'eau et conditions d'existence de la Cédraie dans le Moyen Atlas Basaltique. An. Recher. Forest. Au Maroc. T15. pp : 92 - 269.
43. Termier, H. (1936). Etude *géologique sur le Maroc central et la Moyen Atlas septentrional. Notes et mém. Serv. Géol. Maroc, N°33, 1566p.*
44. Martin, J. (1981). Le Moyen Atlas Central : étude géomorphologique. Thèse d'état, paris 7, Ed. Serv. Géol. Maroc, n° 258. https://www.persee.fr/doc/rga_0035
45. Demirel, Y., & Türk, N. (2024). Automatic detection of active fires and burnt areas in forest areas using optical satellite imagery and deep learning methods. *Mersin Photogrammetry Journal*, 6 (2), 66-78. <https://doi.org/10.53093/mephoj.1575877>
46. Zanchetta, A., Bitelli, G., & Karnieli, A. (2016). Monitoring desertification by remote sensing using the Tasseled Cap transform for long-term change detection. *Nat Hazards* 83:223-237. <https://link.springer.com/article/10.1007/s11069-016-2342-9>
47. Rouse, J. W., Haas R. H., Schell J. A., & Deering D. W. (1973). Monitoring Vegetation Systems in the Great Plains with ERTS. In Paper presented at the Third ERTS Symposium, NASA SP-351, Vol.I, December 10-14, Washington, DC: NASA: 309-317. <https://www.scirp.org/journal/home?journalid=114>
48. Tucker, C. J. (1979). Red and photographic infrared linear combinations for monitoring vegetation. *Remote sensing of Environment*, 8(2), 127-150. [http://dx.doi.org/10.1016/0034-4257\(79\)90013-0](http://dx.doi.org/10.1016/0034-4257(79)90013-0)
49. Zhao, H.L., Li, J., Liu, R.T., Zhou, R.L., Qu, H., & Pan, C.C. (2014). Effects of desertification on temporal and spatial distribution of soil macroarthropods in Horqin sandy grassland, Inner Mongolia. *Geoderma* 223: pp.62-67. <https://doi.org/10.1016/j.GEODERMA.2014.01.026>
50. Ma, Z., Xie, Y., Jiao, J., Wang, X. (2011). The construction and application of an Aledo-NDVI based desertification monitoring model. *Procedia Environ Sci* 10:2029-2035. <https://doi.org/10.1016/j.proenv.2011.09.318>
51. Liang, S., Shuey, C.J., Russ, A.L., & Fang, H. (2003). Narrowband to broadband conversions of land surface albedo: II Validation. *Remote Sensing of Environment* 84 1:25-41 [https://doi.org/10.1016/S0034-4257\(02\)00068-8](https://doi.org/10.1016/S0034-4257(02)00068-8)
52. Qi, J.C., Hehbouni, A., Huete, A.R., Kerr, Y.R., & Sorooshian, S. (1994). A modified soil adjusted vegetation index. ,Volume 48, Issue 2, pp. 119-126. [https://doi.org/10.1016/0034-4257\(94\)9134-1](https://doi.org/10.1016/0034-4257(94)9134-1)
53. Yakar, M. (2011). Using close range photogrammetry to measure the position of inaccessible geological features. *Experimental Techniques*, 35(1), 54-59.
54. Wang, S., Grant, R.F., Versegny, D.L., & Black, T.A. (2002). Modelling carbon dynamics of boreal forest ecosystems using the Canadian Land Surface Scheme. *Clim Change* 55:pp.451-477. <http://doi.org/10.1023/A:1020780211008>
55. Xiao, J., Shen, Y., Tateishi, R., & Bayaer, W. (2006). Development of topsoil grain size index for monitoring desertification in arid land using remote sensing. *Int J Remote Sens* 27:pp. 2411-2422. <http://dx.doi.org/10.1080/01431160600554363>
56. Yakar, M., Yilmaz, H. M., & Yurt, K. (2010). The effect of grid resolution in defining terrain surface. *Experimental Techniques*, 34(6), 23-29.
57. Kauth, R., & Thomas, G. (1976). The tasseled cap a graphic description of the spectral-temporal development of agricultural crops as seen by LANDSAT. LARS symposia. June 29 - July 1, pp. 38-51. https://docs.lib.purdue.edu/lars_
58. Jenks, G.F. (1963). Generalization in statistical mapping. *Ann Assoc Am Geogr* 53:15-26. . [CrossRef]
59. Pan, J., & Li, T. (2013). Extracting desertification from Landsat TM imagery based on spectral mixture analysis and Albedo-Vegetation feature space. *Nat Hazards* 68:915-9 <https://link.springer.com/article/10.1007/s11069-013-0665-3>
60. Gheshlaghi, A.G., Feizizadeh, B., Blaschke, T., Lakes, T., & Tajbar, S. (2020). Forest fire susceptibility modeling using hybrid approaches. *transaction in Gis*, 25(1). <https://doi.org/10.1111/tgis.12688>
61. Yakar, M., Yildiz, F., Uray, F., & Metin, A. (2010, June). Photogrammetric Measurement of The Meke Lake and Its Environment with Kite Photographs to Monitoring of Water Level to Climate Change. In ISPRS Commission V Mid-Term Symposium (pp. 613-616).
62. Da.Silva, T.G.F.d., Cruz Neto, J.F.d., Jardim, A.M.d.R.F., Souza, C.A.A.d., Araújo Júnior, G.d.N., Silva, M.V.d., Silva, J.L.B.d., Carvalho, A.A.d., Montenegro, A.A.d.A., & de Souza, L.S.B. (2024). RisDes_Index: An Index for Analysing the Advance of Areas Undergoing Desertification Using Satellite. *Data. Agri Engineering*, 6, pp.1150-1174. <https://doi.org/10.3390/agriengineering6020066>
63. Wang, G.J., & Zhang, J.C. (2006). Analysis of grassland desertification due to coal mining based on remote sensing - An example from huolinhe open-cast coalmine. *Journal of China University of Mining and Technology*, 10(6),

- 917-25.
<https://dx.doi.org/10.11834/jrs.200606134>
64. Djeddaoui, F., Chadli, M., & Gloaguen, R. (2017). Desertification Susceptibility Mapping Using Logistic Regression Analysis in the Djelfa Area, Algeria, *Remote Sensing*. 2017, 9(10), 1031. <https://doi.org/10.3390/rs9101031>
 65. Benslimane, M., Hamimed, A., Elzerey, W., Khaldi, A., & Mederbal, K. (2021). Analyse et suivi du phénomène de la désertification en Algérie du nord, *Vertigo* 8(3):Ppp.1-97. <https://doi.org/10.4000/vertigo.6782>
 66. Mihi, A., Ghazela, R., & Wissal, D. (2022). Mapping potential desertification-prone areas in North-Eastern Algeria using logistic regression model, GIS, and remote sensing techniques. *Environmental Earth Sciences*. <https://www.researchgate.net/publication/362193731>
 67. Elkhabaz, M., Boumaaza, T., & Aoughar, M. (2024). Modélisation spatiale du phénomène de désertification par l'approche MEDALUS dans le Bassin Central de la Moulouya, *Questions, théories et méthodologies en sciences humaines et sociales Publications du Faculté des lettres et des Sciences Humaines, Mohammadia*. pp. 68-88.
 68. Crist, E.P. Laurin, R., & Cicone, R.C. (1986). Vegetation and Soils Information Contained in Transformed Thematic Mapper Data. *Proceedings of International Geoscience and Remote Sensing 86 Symposium, Zurich, Switzerland*. <https://www.scirp.org/reference/referencespapers?referenceid=2089836>
 69. Lamchin, M., Lee, J.Y., Lee, W.K., Lee, E.J., Moonil, K., Lim, C.H.A., Choi, H.A.b., & Kim, S.R. (2016). Assessment of land cover change and desertification using remote sensing technology in a local region of Mongolia. *Adv Sp Res* 57:64.
 70. Eyi, G., & Buğdaycı, İ. (2024). Uzaktan algılama yöntemleri ile yangın şiddetinin tespiti: Yunanistan Rodos Adası orman yangını örneği. *Geomatik*, 9(3), 348-360. <https://doi.org/10.29128/geomatik.1481708>
 71. Yakar M, Yılmaz H M & Mutluoğlu Ö (2010). Comparative evaluation of excavation volume by TLS and total topographic station based methods. *Lasers in Eng*, 19, 331-345.
 72. Ünel, F. B., Kuşak, L., Yakar, M., & Doğan, H. (2023). Coğrafi bilgi sistemleri ve analitik hiyerarşi prosesi kullanarak Mersin ilinde otomatik meteoroloji gözlem istasyonu yer seçimi. *Geomatik*, 8(2), 107-123. <https://doi.org/10.29128/geomatik.1136951>



© Author(s) 2026. This work is distributed under <https://creativecommons.org/licenses/by-sa/4.0/>